

Cite this article as: Wang Yunlei, Ren Liping, Dong Jingren, et al. Grain Size Prediction and Growth Thermo-Kinetics Analysis During Annealing with Different Heating Rates for High-Voltage Anode Aluminum Foil[J]. Rare Metal Materials and Engineering, 2022, 51(06): 2020-2026.

ARTICLE

Grain Size Prediction and Growth Thermo-Kinetics Analysis During Annealing with Different Heating Rates for High-Voltage Anode Aluminum Foil

Wang Yunlei¹, Ren Liping¹, Dong Jingren¹, Cao Chuanchuan^{2,3}, Liu Xun⁴, Jiang Pan⁴

¹ School of Materials Science and Engineering, Chongqing University of Arts and Sciences, Chongqing 402160, China; ² School of Intelligent Manufacturing Engineering, Chongqing University of Arts and Sciences, Chongqing 402160, China; ³ School of Energy and Power Engineering, Lanzhou University of Technology, Lanzhou 730050, China; ⁴ China Merchants New Material Technology (Chongqing) Co., Ltd, Chongqing 402160, China

Abstract: Based on electron backscattered diffraction (EBSD) and grain growth model of thin film materials, grain sizes and growth thermo-kinetics were investigated during annealing with different heating rates in high-voltage anode aluminum foil. Results show that the grain growth exponent $n=4$, activation energy $Q_g=129$ kJ/mol and rate constant $K=1.28\times 10^{-8}$ m⁴·s⁻¹ are calculated by the typical isothermal grain growth equation. Based on grain growth model of thin film materials and energy anisotropy, the reasons for the rapid growth of (001) oriented grains are well explained, and a typical $40^\circ<111>$ misorientation relationship with S-grains is found.

Key words: high-voltage anode aluminum foil; heating rate; grain growth model; grain size; thermo-kinetics

In scientific research, the grain sizes and growth thermo-kinetics play an important role in revealing the microstructures evolution during annealing process of metallic materials^[1-4]. In particular, the cube grain growth and its size evolution in high-voltage anode aluminum foil^[5-7], and the capacitance of the electrolytic capacitor depend on the surface of the aluminum foil. Therefore, understanding and regulating the development of the microstructures and textures of aluminum foil will help to control and eventually improve the capacitance and properties of high-voltage anode aluminum foil.

High-level cold rolling of aluminum foil always undergoes final annealing and obtains large-sized cube component^[6, 8-10]. However, the abnormal grain growth behavior is obviously and commonly observed in annealing foil. The cube texture plays a significant role and acts as a typical recrystallization texture to control the microstructures of aluminum foil, which seriously affects the capacitance of the electrolytic capacitor; based on the influence of cube texture on qualities of aluminum foil, the evolution of microstructures and textures

are investigated in rapid annealing process with different heating rates. In the previous studies, influence of heating rate on the initiation of primary recrystallization in a deformed Al-Mg alloy was studied by Attallah^[11], who suggested the recrystallization behavior at different heating rates. Ferry et al^[12] studied the influence of rapid heating rate on recrystallization nucleation and final grain size in particle-containing aluminum alloys. However, the effect of different heating rates on cube texture and abnormal grain growth during rapid annealing in high-voltage anode aluminum foil was rarely reported.

It is the goal of the present study to investigate the effect of heating rates on abnormal grain growth behavior. Analysis was conducted on the details of growth thermo-kinetics in high-voltage anode aluminum foil during rapid annealing. It is based on the grain growth model of thin film materials and energy anisotropy to calculate activation energy and grain growth rates. The cube texture in high purity aluminum foils was examined, which were produced with a high degree of

Received date: June 23, 2021

Foundation item: University-level Project Funding (2017RCH01); Science and Technology Research Program of Chongqing Municipal Education Commission (KJQN202001301)

Corresponding author: Wang Yunlei, Ph. D., Lecturer, School of Materials Science and Engineering, Chongqing University of Arts and Sciences, Chongqing 402160, P. R. China, Tel: 0086-23-49855073, E-mail: wangyunlei@cqu.edu.cn

Copyright © 2022, Northwest Institute for Nonferrous Metal Research. Published by Science Press. All rights reserved.

cold reduction (without inter-annealing) and a proper finishing temperature. The evolution of (001) oriented grains or cube texture, grain size during rapid annealing of the cold rolled foils were tracked by investigations of microstructures and crystallographic textures.

1 Experiment

High purity aluminum sheet was subjected to a high level of cold rolling to 0.11 mm with a 99% reduction and more than 20 passes without inter-annealing. The final thickness of 0.11 mm aluminum foil was considered as a thin film and was used for further analysis. Subsequently, the cold reduction of 99% high purity aluminum foil was annealed at different peak temperatures from 400 °C to 500 °C, and the temperature rising from room temperature to peak temperature in this annealing process was controlled by different heating rates. The samples were heated to the target temperatures, and then rapidly cooled in water to room temperature. The detailed schematic of cold rolling and annealing process is plotted in Fig.1.

The microstructures and textures were characterized by the optical microscopy (using by polarized light) and EBSD (HKL/Channel 5) technique. For the thin aluminum foil areas of 450 μm \times 550 μm , they were scanned by steps of 0.8 μm , so the maps were composed of some 300 000 data points. The results of microstructures, orientation topographies, grain sizes, etc will be analyzed and discussed in Section 2 and Section 3.

2 Results

2.1 Abnormal growth behavior

Abnormal growth behavior^[13-15] is obviously observed in high-level cold rolling and subsequent annealing in air furnace. After the annealing, in order to reveal the grain structure, the samples were etched in a solution of 50 mL HF, 47 mL HNO₃ and 3 mL HF for 1~3 min. The microstructures of high purity aluminum foil after etching are shown in Fig.2, which shows that large recrystallization grains (RX grain) form after annealing at 500 °C for 20 and 600 s. Apart from

these large recrystallization grains, there are still some sub-grains in Fig.2a, and the mean grain size is 200~400 μm , the average size of 300~500 grains is checked by optical microscopy image analyzing and polarization contrast. However, it obtains a fully recrystallized structure without a deformed matrix when the annealing time rises to 600 s (Fig.2b), and the most important feature of grain growth in this rapid annealing process is changed from normal grain growth to abnormal grain growth, and the individual abnormal grain size approximates to millimeter-size.

2.2 Microstructure development during annealing

Completely different microstructures are generated in samples when heated in Gleeble-1500 thermal cycling to the peak temperature (500 °C) with different heating rates (Fig.3). Annealing over the range of heating rates (up to 50 °C/s) is studied, and the microstructures are obtained by carefully using electrolytic polishing and anodic coating and polarized light of the Axiovert 40MAT optical microscopy. Fig. 3 exhibits an obvious variation of grain structures and grain sizes with changing the heating rates. When the heating rates increase from 0.5 °C/s to 10 °C/s, a 100% fraction of fully recrystallized grain structures are obtained, as shown in Fig. 3a~3d. However, at a higher heating rate of 25 °C/s, the sample shows a small fraction of recrystallized grains (5%~10%) within the deformed structures as shown in Fig. 3e. When the heating rate is up to 50 °C/s, the recrystallization does not appear but some small recrystallization nuclei come into being, which indicates that the microstructure is a complete recovery structure (Fig. 3f). The effect of heating rates on recrystallized volume fractions and grain sizes has been studied in previous work^[11,16-18]. The heating rate is an important factor in controlling the annealing process, which is used to control the cube texture and other component in high-voltage anode aluminum foil, and to improve the surface quality of aluminum foil.

3 Discussion

3.1 Grain size calculation

The grain sizes and their growth rates are of great practical

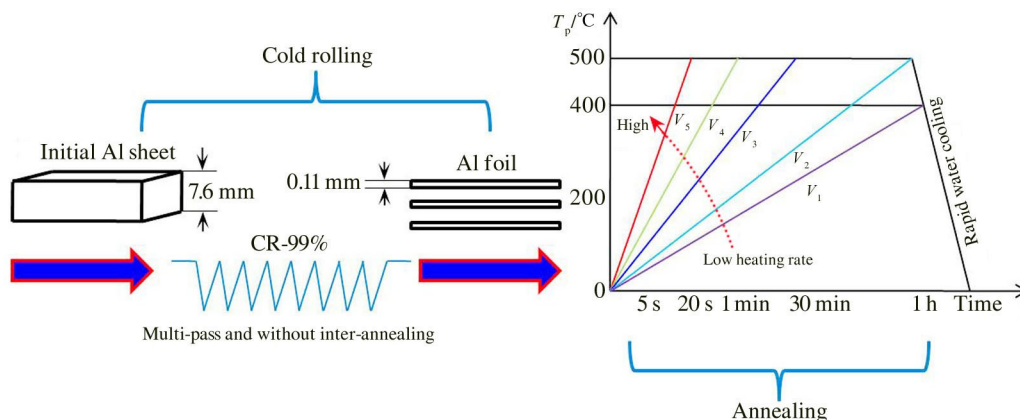


Fig.1 Schematic of aluminum sheet during cold rolling and annealing process

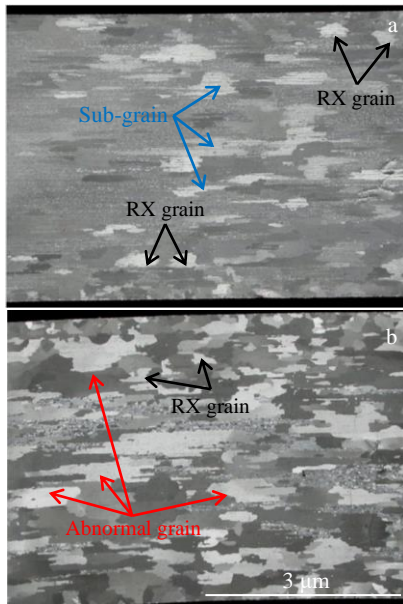


Fig.2 Microstructures of high purity aluminum foil after acid etching during rapid annealing at 500 °C for 20 s (a) and 600 s (b)

significance in metal materials. However, the modifications of a classical model of grain growth during isothermal heating was proposed by Murty^[19], and typical isothermal grain growth equation of metal materials is drawn as follows:

$$D^n - D_0^n = Kt \exp\left(-Q_g/RT\right) \quad (1)$$

where D and D_0 denote the initial and final grain sizes, respectively; T and t are annealing temperature and time, respectively; n , K , and Q_g represent the grain growth exponent, rate constant, and activation energy, respectively; R is the gas constant.

In order to analyze the isothermal heating process, both sides of Eq. (1) are differentiated to study grain growth kinetics:

$$d(D^n) = K \left(\exp\left(-Q_g/RT\right) \right) dt \quad (2)$$

Eq. (2) represents the increment of grain growth in a short time or a short period of temperature range. Assuming that the heating rate $v=dT/dt$, and substituting it into Eq.(2), we get the isothermal grain growth equation:

$$D^n - D_0^n = \frac{K}{v} \int_{T_i}^{T_f} \exp\left(-Q_g/RT\right) dT \quad (3)$$

where T_i and T_f denote the recrystallization start temperature and peak temperature, and the calculation accuracy of grain sizes prediction will be improved by Eq.(3).

For a constant heating rate, $v=dT/dt$, Eq.(3) is integrated by Bourell et al^[20] to obtain an expression for D in terms of an infinite series in the variable $\exp(-Q_g/RT)$. As suggested by Bourell, for $T_f \gg T_i$, where T_i and T_f are the initial and peak temperature, respectively, this series can be truncated to the following form without the introduction of substantial errors:

$$D^n - D_0^n = \frac{KR}{vQ_g} \left[T_f^2 \exp\left(-Q_g/RT_f\right) - T_i^2 \exp\left(-Q_g/RT_i\right) \right] \quad (4)$$

Eq.(4) suggests that it can calculate the parameters of n and Q_g during recrystallization. And $v(D^n - D_0^n)$ is a constant when T_f and T_i are the same in annealing. Therefore, n is calculated as follows:

$$n = \frac{\ln(v_2/v_1)}{\ln\left[(D_{f1} - D_0)/(D_{f2} - D_0)\right]} \quad (5)$$

In our experiments, $v_1=10$ °C/s, $v_2=25$ °C/s, $D_0=10$ μm, $T_{f1}=400$ °C, $T_{f2}=500$ °C, $D_{f1}=78$ μm, $D_{f2}=65$ μm; thus we get $n=3.8$, which approaches the value of 4 and is proposed by Humphreys et al^[21]; in order to calculate conveniently, we

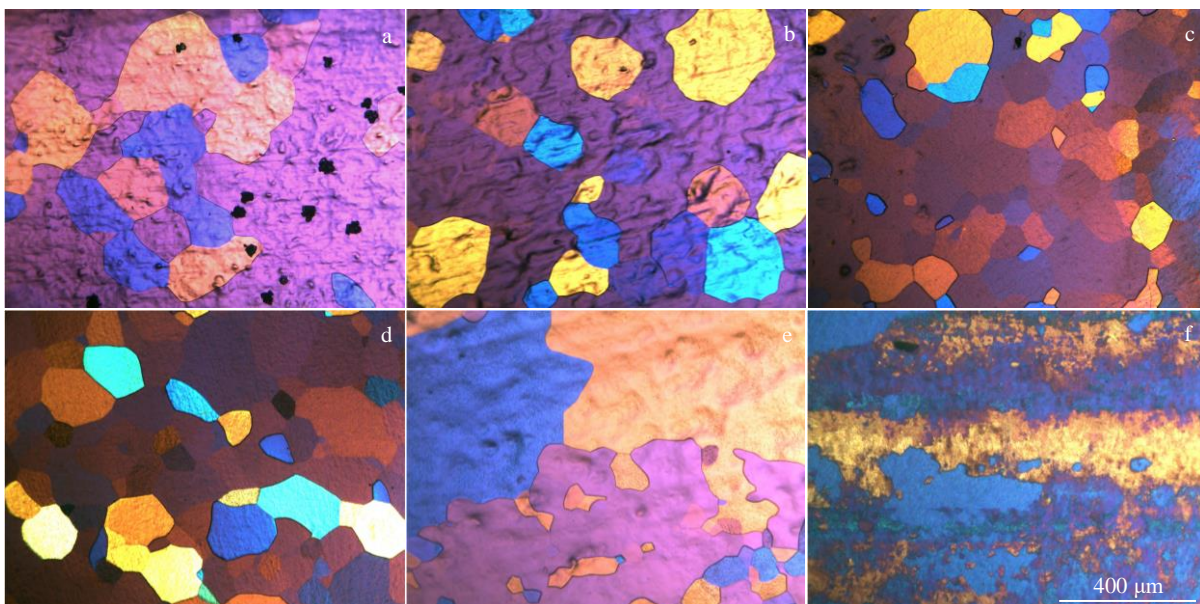


Fig.3 Microstructures heated from room temperature to 500 °C at various heating rates: (a) 0.5 °C/s, (b) 1.0 °C/s, (c) 5.0 °C/s, (d) 10 °C/s, (e) 25 °C/s, and (f) 50 °C/s

assume $n=4$. Using the geometric relationship, and selecting D_1, D_2 for fixed values of final grain size D , Eq. (4) can be applied to estimate Q_g . In order to simplify the estimation, the exponential term in T_i can be neglected. For typical activation energies, this corresponds generally to $T_i \geq T_i + 200$. In these cases, Eq.(4) becomes:

$$Q_g = \frac{R \left[n \ln \frac{D_2}{D_1} + \ln \frac{v_2}{v_1} - 2 \ln \frac{T_{r2}}{T_{r1}} \right]}{1/T_{r1} - 1/T_{r2}} \quad (6)$$

As known from experimental data including $D_1=185 \mu\text{m}$, $D_2=61 \mu\text{m}$, $v_1=10 \text{ }^\circ\text{C/s}$, $v_2=25 \text{ }^\circ\text{C/s}$, $T_{r1}=773 \text{ K}$, $T_{r2}=673 \text{ K}$, $R=8.314 \text{ J}\cdot\text{mol}^{-1}\cdot\text{K}^{-1}$, $n=4$, we can calculate parameters of $Q_g=129 \text{ kJ/mol}$ and $K=1.28 \times 10^{-8} \text{ m}^4\cdot\text{s}^{-1}$.

The grain sizes of annealing are obtained by the calculated values of material constants ($n=4$, $Q_g=129 \text{ kJ/mol}$, and $K=1.28 \times 10^{-8} \text{ m}^4\cdot\text{s}^{-1}$) combined with Eq.(1). A series of calculated grain sizes and variation tendency at the annealing peak temperatures (400 and 500 °C) are plotted in Fig. 4, which indicates that there are some errors between calculated values and experimental data, the deviation of grain sizes is relatively small when the heating rates increase to 10 °C/s. While heating rate is beyond 10 °C/s, the deviation of grain sizes is relatively large between calculated values and experimental data; this is because a higher heating rate does not provide sufficient time for these deformed structure to transform into recrystallized grain. Therefore, in this case, it consists of deformed grains and recrystallized grains, which affect the measurement of grain sizes. Actually, the calculated values of grain size D acts as a function of heating rate v and T , which provides a certain theoretical foundation in industrial application, so it will obtain a grain size quickly for practical

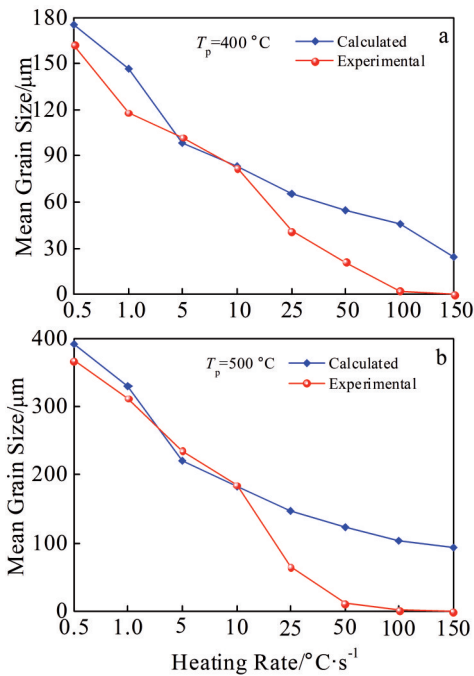


Fig.4 Mean grain size of calculated and experimental value with different heating rates at $T_p=400 \text{ }^\circ\text{C}$ (a) and $T_p=500 \text{ }^\circ\text{C}$ (b)

production without some experiments, which saves the cost in a certain extent.

3.2 Thermo-kinetics analysis of grain growth

Aluminum foil is considered as a thin foil with columnar grains which are distributed along the thickness direction (<001>/ND). And the detailed model is shown in Fig.5. It is a model of demonstrated thin film which is deposited on a substrate. The effect of energy anisotropy^[22] on abnormal grain growth is studied, and a new development of this model for thin aluminum foil is conducted in present experiment.

Therefore, it is assumed that L is thin foil thickness, R_n is mean grain size, $\bar{\gamma}_s, \bar{\gamma}_i, \bar{\gamma}_w$ are average surface energy density, interface energy density and strain energy density, respectively, R_a is abnormal grain size.

So before the abnormal grain growth, P_1 is the total energy density of this area.

$$P_1 = \frac{\pi R_a^2 \bar{\gamma}_s + \pi R_a^2 \bar{\gamma}_i + \pi R_a^2 L \bar{\gamma}_w + 2\pi R_a L N_n A_{GB} \gamma_{GB}}{\pi R_a^2 L} \quad (7)$$

While this area transforms into an abnormal grain, the total energy density of this area becomes P_2 .

$$P_2 = \frac{\pi R_a^2 \gamma_s + \pi R_a^2 \gamma_i + \pi R_a^2 L \gamma_w + 2\pi R_a L \gamma_{GB}}{\pi R_a^2 L} \quad (8)$$

where N_n is the number of normal grains per unit volume, A_{GB} is the average grain boundary area in a single normal grain. Therefore, the energy density variation is:

$$\Delta P = P_2 - P_1 = -\frac{\Delta \gamma_s}{L} - \frac{\Delta \gamma_i}{L} - \Delta \gamma_w + \frac{2\gamma_{GB}}{R_a} - N_n A_{GB} \gamma_{GB} \quad (9)$$

The normal columnar grain shape is considered as a regular hexagonal prism, so the N_n, A_{GB} can be written:

$$\left. \begin{aligned} N_n &= \frac{1}{V_n} = \frac{2}{3\sqrt{3} R_n L} \\ A_{GB} &= \frac{6R_n L}{2} = 3R_n L \end{aligned} \right\} \quad (10)$$

Eq.(9) can be deduced:

$$\Delta P = -\frac{\Delta \gamma_s}{L} - \frac{\Delta \gamma_i}{L} - \Delta \gamma_w + \frac{2\gamma_{GB}}{R_a} - \frac{1.15\gamma_{GB}}{R_n} \quad (11)$$

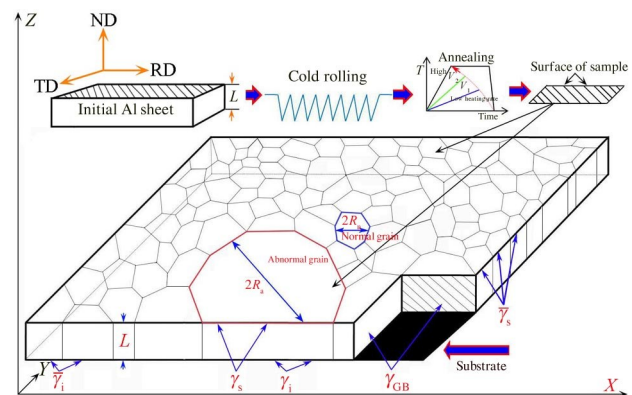


Fig.5 Model of abnormal grain growth under controlled energy anisotropy in thin film

Before the abnormal grain is impeded or piled up, grain

$$\frac{dR_a}{dt} = -M(T) \cdot \Delta P = \frac{D_0}{RT} \exp\left(-\frac{Q_g}{RT}\right) \cdot \left(\frac{\Delta\gamma_s}{L} + \frac{\Delta\gamma_i}{L} + \Delta\gamma_w + \frac{1.15\gamma_{GB}}{R_n} - \frac{2\gamma_{GB}}{R_a}\right) \quad (12)$$

Eq.(12) suggests that the grain growth rate depends on two determinants. Kinetics is the activity of the grain boundary (i.e., dynamics condition). Thermodynamics is a driving force of grain boundary migration (i.e., thermodynamic conditions).

In our present study, the thin aluminum foil is a free film, so $\Delta\gamma_s = \Delta\gamma_b$, $\Delta\gamma_w = 0$, Eq.(12) is conducted as:

$$\frac{dR_a}{dt} = M(T) \cdot \left(\frac{2\Delta\gamma_s}{L} + \frac{1.15\gamma_{GB}}{R_n} - \frac{2\gamma_{GB}}{R_a}\right) \quad (13)$$

Eq.(13) indicates three aspects of driving force for grain growth. The first one is energy anisotropy (surface energy, grain boundary energy), which acts as a driving force for abnormal grain growth; the second one is a driving force which is generated as the normal grain boundary areas decrease; the third one is the generated resistance which is accompanied with the abnormal grain boundary areas increasing.

In order to investigate energy anisotropy which acts as a driving force for abnormal grain growth, the samples are subjected to rapid annealing at 500 °C for 10 and 60 s, and (001) oriented grains are analyzed in Fig.6.

3.3 Analysis of (001) oriented grain

Typical development of grain structure after peak temperature (500 °C) annealing for 10 s is shown in Fig. 6. These selected 12 red grains are (001) oriented grains^[23], which have preferential and rapid growth within the main (111) oriented matrix (blue area or grains, shown in Fig. 6a), and some individual grains rapidly grow and develop into recrystallized grains. However, the abnormal grain growth behavior (Fig.6b) appears while the annealing time is up to 60 s. Specifically, a large scale grain size is beyond 110 μm (thickness of aluminum foil), these grains grow more quickly than other neighboring grains, and these fully recrystallized grains deviate from the equilibrium position compared with the position in ideal {111} pole figure.

In fcc systems, a 30°~40° <111> misorientation relationship

growth rate of this abnormal grain in thin foil is written as:

is often attributed to the high growth rate. And in fact, the cube orientation ({001} <100>) has a misorientation relationship with S-component ({123} <634>) of the deformation texture. In order to explore the orientation relationship between cube and S-texture, we select the independent oriented grains during annealing at 500 °C for 60 s, and the {111} pole figure exhibits the typical 40° <111> misorientation relationship between cube and S-texture (Fig. 7). However, cube grains have the best chance of growing, because this particular orientation makes the best “compromise” toward meeting the 40° <111> misorientation relationship with S-component, which has been argued by Eddahbi et al^[24]. This result well explains why the cube grains have a high growth rate (Fig. 6, corresponding to (001) oriented grains) during rapid annealing after high-level cold reductions.

3.4 (001) oriented grain growth rate

In fact, the new essentially perfect recrystallization nuclei develop and grow at the expense of deformed matrix via the migration of recrystallization grain boundaries. The migration rate V is usually expressed as follows:

$$V = M(T) \cdot \Delta P \quad (14)$$

$$M(T) = M_0 \exp\left(-\frac{Q_g}{RT}\right) \quad (15)$$

According to Eq.(15), by adopting the constant $M_0=7.8 \times 10^{-7} \text{ m}\cdot\text{s}^{-1}\cdot\text{Pa}^{-1}$ in previous study of Rahman^[25] in high purity aluminum and calculated values of $Q_g=129 \text{ kJ/mol}$ in the above discussion, the calculated value of grain boundaries mobility M acts as a function of temperature T , which is shown in Table 1. The grain boundaries mobility M is $1.49 \times 10^{-15} \text{ m}\cdot\text{s}^{-1}\cdot\text{Pa}^{-1}$ at 500 °C.

The section of thermo-kinetics analysis of grain growth indicates that energy anisotropy (surface energy, grain boundary energy) acts as a driving force^[22,26-28] for abnormal

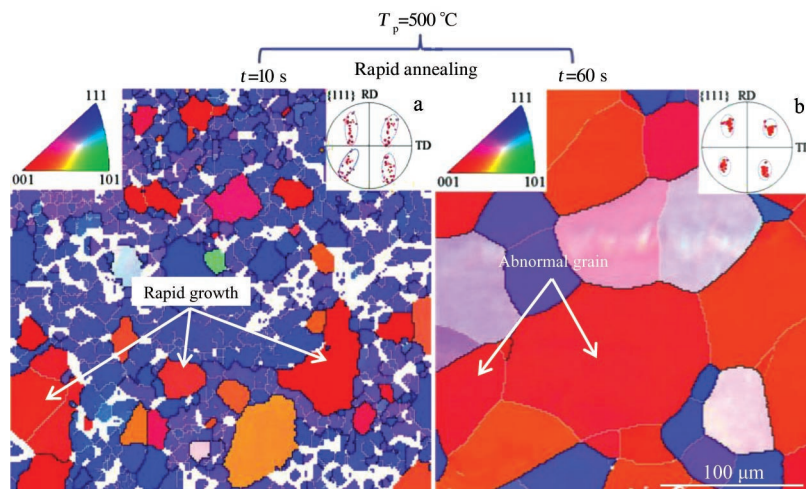


Fig.6 {111} pole figure (a) and orientation imaging microscopy analysis (b) of selected grains during rapid annealing

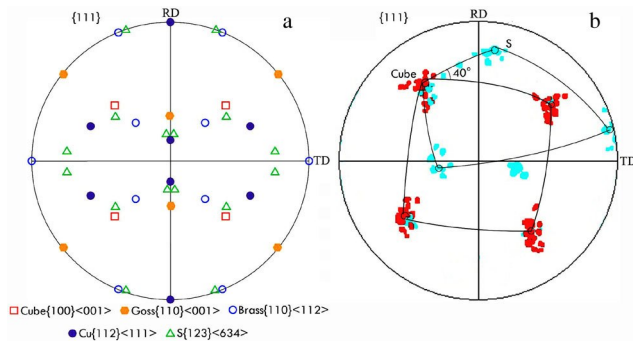


Fig.7 Misorientation relationship of $40^\circ\langle 111\rangle$ between cube and S-component annealed at 500°C for 60 s (a) and cube component transformed from 10 s to 60 s (b)

Table 1 Calculated value of grain boundary mobility M as a function of temperature T

Temperature/ $^\circ\text{C}$	350	400	450	500
$M/\text{m}\cdot\text{s}^{-1}\cdot\text{Pa}^{-1}$	1.19×10^{-17}	7.61×10^{-17}	3.73×10^{-16}	1.49×10^{-15}

grain growth, and if we combine it with Fig. 6, we can conclude that the (001) oriented grains have the advantage of higher growth rate than other deformed grain, and these (001) oriented grains have been identified as cube component. Therefore, grain growth rate V_{gg} is expressed as follows:

$$V_{\text{gg}} = M(T) \cdot \left(\frac{2\Delta\gamma_{(001)}}{L} + \frac{1.15\gamma_{\text{GB}}}{R_n} - \frac{2\gamma_{\text{GB}}}{R_a} \right) \quad (16)$$

Based on Eq. (16), the effect of parameters or edge conditions on grain growth rate (V_{gg}) during annealing process is discussed. Therefore, two aspects are shown.

(1) In the initial stage of abnormal grain growth, $R_a \approx R_n$, V_{gg} is expressed as follows:

$$V_{\text{gg}} = M(T) \cdot \left(\frac{2\Delta\gamma_{(001)}}{L} - \frac{0.85\gamma_{\text{GB}}}{R_n} \right) \quad (17)$$

(2) In the later stage of the abnormal grain growth, its size is much bigger than the surrounding normal grain size, $R_a \gg R_n$, V_{gg} is expressed as follows:

$$V_{\text{gg}} = M(T) \cdot \left(\frac{2\Delta\gamma_{(001)}}{L} + \frac{1.15\gamma_{\text{GB}}}{R_n} \right) \quad (18)$$

However, we assume that the surface energy anisotropy is considered as the only driving force for abnormal grain growth, and it is the typical mechanism of surface energy inducing abnormal grain growth in thin aluminum foil. In fcc systems, in general, the (111) has a minimum surface energy. Therefore, while any crystal-planes (hkl) act as a surface, we can roughly estimate the surface energy of these crystal-planes (hkl) by calculating the included angle between any crystal-plane (hkl) and (111). In this experiment, the included angle is $\theta=54.74^\circ$ between (001) and (111), and Zhang^[28] has calculated that $\gamma_{(001)}=898\text{ mJ/m}^2$, $\gamma_{(111)}=619\text{ mJ/m}^2$ in aluminum. So based on Eq.(16) and ignoring the grain boundary energy γ_{GB} , the grain growth rates V_{gg} are calculated and shown in Table 2. It is obvious that the grain growth rate $V_{\text{gg}}=2.43\times 10^{-2}\mu\text{m}\cdot\text{s}^{-1}$ at

Table 2 Calculated value of grain growth rate V_{gg} as a function of temperature T

Temperature/ $^\circ\text{C}$	350	400	450	500
$V_{\text{gg}}/\mu\text{m}\cdot\text{s}^{-1}$	1.94×10^{-4}	1.24×10^{-3}	6.09×10^{-3}	2.43×10^{-2}

the temperature of 500°C , and this grain growth rate is relatively higher in thin aluminum foil than in bulk materials during rapid annealing at 500°C . Therefore, it well explains the cause for quick growth of (001) oriented grains.

4 Conclusions

1) The grain sizes can be effectively predicted by typical isothermal grain growth equations, and the values of material constants can also be calculated ($n=4$, $Q_g=129\text{ kJ/mol}$, and $K=1.28\times 10^{-8}\text{ m}^4\cdot\text{s}^{-1}$). The investigated high-voltage anode aluminum foils during rapid annealing are in good agreement with experimental results.

2) Based on energy anisotropy, the model of abnormal grain growth in thin aluminum foil is established, which analyzes the growth thermo-kinetics during rapid annealing at the temperature of 500°C .

3) The (001) oriented grains have higher growth rate than other deformed grains, because the cube grains of (001) orientation meet the typical $40^\circ\langle 111\rangle$ misorientation relationship with S-grains. And while the crystal-plane (001) is considered as a surface, the grain growth rate V_{gg} is calculated as $2.43\times 10^{-2}\mu\text{m/s}$ at 500°C .

References

- 1 Rohrer G S, Li J, Lee S et al. *Materials Science and Technology* [J], 2010, 26 (6): 661
- 2 Cordier P, Demouchy S, Beausir B et al. *Nature*[J], 2014, 507 (7490): 51
- 3 Qiu C Y, Li L, Hao L L. *International Journal of Minerals, Metallurgy, and Materials*[J], 2018, 25: 536
- 4 Azzeddine H, Abdessameud S, Alili B et al. *Bulletin of Materials Science*[J], 2011, 34(7): 1471
- 5 Peng N, Wen Y Q, Shang W et al. *Journal of Materials Science* [J], 2020, 55(3): 1246
- 6 Bodakin L, Gusakov A, Komarov O et al. *Technical Physics*[J], 2016, 61(9): 1404
- 7 Chen T, Guo Z, Zeng B et al. *International Journal of Advanced Manufacturing Technology*[J], 2017, 93(9-12): 3275
- 8 Kumar A, Gupta A, Khatirkar R K et al. *Philosophical Magazine Letters*[J], 2018, 98(1): 17
- 9 Pan F S, Peng J, Tang A et al. *Materials Science and Technology* [J], 2005, 21(12): 1432
- 10 Jin H. *Materials Science and Technology*[J], 2011, 27(3): 702
- 11 Attallah M M, Strangwood M, Davis C L. *Scripta Materialia*[J], 2010, 63(4): 371
- 12 Ferry M, Jones D. *Scripta Materialia*[J], 1997, 38(2): 177
- 13 Umakoshi Y, Matsumoto K, Shibayanagi T et al. *Materials and*

- Design* [J], 1997, 18(4-6): 227
- 14 Rheinheimer W, Hoffmann M J. *Journal of Materials Science*[J], 2016, 51(4): 1756
- 15 Wang C M, Chan H M, Harmer M P. *Journal of the American Ceramic Society*[J], 2004, 87(3): 378
- 16 Xia S L, Ma M, Zhang J X et al. *Materials Science and Engineering A*[J], 2014, 609(15): 168
- 17 Li P, Li J, Meng Q. *Ironmaking and Steelmaking*[J], 2015, 42(2): 81
- 18 Primig S, Leitner H, Clemens H et al. *International Journal of Refractory Metals and Hard Materials*[J], 2010, 28(6): 703
- 19 Murty H N. *Philosophical Magazine*[J], 1969, 20 (166): 855
- 20 Bourell D L, Parimal, Kaysser W. *Journal of the American Ceramic Society*[J], 1993, 41: 2933
- 21 Humphreys F J, Hatherly M. *Recrystallization and Related Annealing Phenomena*[M]. New York: Pergamon, 2004
- 22 Zhang J M, Ma F, Xu K W et al. *Surface and Interface Analysis* [J], 2003, 35: 805
- 23 Sonnweber-Ribic P, Gruber P A, Dehm G et al. *Acta Materialia* [J], 2012, 60(5): 2397
- 24 Eddahbi M, Carsí M, Ruano O A. *Journal of Materials Science* [J], 2006, 41: 5576
- 25 Rahman M J, Zurob H S, Hoyt J J. *Acta Materialia*[J], 2014, 74(1): 39
- 26 Yao X, Zhang Z, Zheng Y F. *Journal of Materials Science and Technology*[J], 2017, 33(9): 1023
- 27 Li W, Chu Z B, Wang H Z et al. *Rare Metal Materials and Engineering*[J], 2020, 49(12): 4088
- 28 Zhang J M, Ma F, Xu K W. *Applied Surface Science*[J], 2004, 229(1-4): 34

高纯铝箔在不同退火加热速率下的晶粒尺寸预测及生长动力学分析

王运雷¹, 任莉平¹, 董井忍¹, 曹川川^{2,3}, 刘 洵⁴, 蒋 攀⁴

(1. 重庆文理学院 材料科学与工程学院, 重庆 402160)

(2. 重庆文理学院 智能制造工程学院, 重庆 402160)

(3. 兰州理工大学 能源与动力工程学院, 甘肃 兰州 730050)

(4. 招商局新材料科技(重庆)有限公司, 重庆 402160)

摘要: 基于电子背散射衍射技术 (EBSD) 和薄膜材料晶粒生长模型理论, 对高压阳极铝箔在不同升温速率下退火的晶粒尺寸及其生长动力学进行了研究。结果表明: 依据典型的等温晶粒生长方程, 可以计算得出晶粒生长指数 $n=4$, 活化能 $Q_g=129$ kJ/mol, 速率常数 $K=1.28 \times 10^{-8} \text{ m}^4 \cdot \text{s}^{-1}$ 。基于薄膜材料的晶粒生长模型和能量各向异性特性, 解释了 (001) 取向晶粒得以快速生长的原因, 且发现这些快速生长的晶粒与 S 晶粒呈 $40^\circ < 111 >$ 取向关系。

关键词: 高压阳极铝箔; 加热速率; 晶粒生长模型; 晶粒尺寸; 热力学

作者简介: 王运雷, 男, 1985年生, 博士, 讲师, 重庆文理学院材料科学与工程学院, 重庆 402160, 电话: 023-49855073, E-mail: wangyunlei@cqu.edu.cn